

Article

Artificial Neural Network Assisted Variable Step Size Incremental Conductance MPPT Method with Adaptive Scaling Factor

Song-Pei Ye, Yi-Hua Liu * , Chun-Yu Liu , Kun-Che Ho and Yi-Feng Luo 

Department of Electrical Engineering, National Taiwan University of Science and Technology, Taipei 106335, Taiwan; D10807202@mail.ntust.edu.tw (S.-P.Y.); D10607002@mail.ntust.edu.tw (C.-Y.L.); D10507001@mail.ntust.edu.tw (K.-C.H.); YF.Luo@mail.ntust.edu.tw (Y.-F.L.)

* Correspondence: yhliu@mail.ntust.edu.tw

Abstract: In conventional adaptive variable step size (VSS) maximum power point tracking (MPPT) algorithms, a scaling factor is utilized to determine the required perturbation step. However, the performance of the adaptive VSS MPPT algorithm is essentially decided by the choice of scaling factor. In this paper, a neural network assisted variable step size (VSS) incremental conductance (IncCond) MPPT method is proposed. The proposed method utilizes a neural network to obtain an optimal scaling factor that should be used in current irradiance level for the VSS IncCond MPPT method. Only two operating points on the characteristic curve are needed to acquire the optimal scaling factor. Hence, expensive irradiance and temperature sensors are not required. By adopting a proper scaling factor, the performance of the conventional VSS IncCond method can be improved, especially under rapid varying irradiance conditions. To validate the studied algorithm, a 400 W prototyping circuit is built and experiments are carried out accordingly. Comparing with perturb and observe (P&O), α -P&O, golden section and conventional VSS IncCond MPPT methods, the proposed method can improve the tracking loss by 95.58%, 42.51%, 93.66%, and 66.14% under EN50530 testing condition, respectively.

Keywords: neural network; variable step size; maximum power point tracking; incremental conductance method



Citation: Ye, S.-P.; Liu, Y.-H.; Liu, C.-Y.; Ho, K.-C.; Luo, Y.-F. Artificial Neural Network Assisted Variable Step Size Incremental Conductance MPPT Method with Adaptive Scaling Factor. *Electronics* **2022**, *11*, 43. <https://doi.org/10.3390/electronics11010043>

Academic Editor: Gianpaolo Vitale

Received: 6 October 2021

Accepted: 20 December 2021

Published: 23 December 2021

Publisher's Note: MDPI stays neutral with regard to jurisdictional claims in published maps and institutional affiliations.



Copyright: © 2021 by the authors. Licensee MDPI, Basel, Switzerland. This article is an open access article distributed under the terms and conditions of the Creative Commons Attribution (CC BY) license (<https://creativecommons.org/licenses/by/4.0/>).

1. Introduction

Solar power generation (SPG) has become one of the most valuable green energy sources due to its advantages of cleanliness, safety, non-pollution, inexhaustibility, and no need for rotating components in the process of assembly and operation. Moreover, solar power generation systems (SPGSSs) are also widely accepted and used in remote areas because of their easy installation [1–3]. However, solar power generation systems are expensive, and changes in irradiance level and ambient temperature will affect their power output. Hence, many scholars have studied how to increase generation efficiency so that these systems can output the maximum available power. Although numerous maximum power point tracking (MPPT) methods have been proposed in the literature, the traditional MPPT technologies, such as hill-climbing, the perturbation and observation method (P&O), and the incremental conductance method (IncCond), are still the most easily implemented and most widely used algorithms [4,5]. The main problem of the traditional MPPT methods is the tradeoff of the perturbation step size (PSS) during the MPPT process because the PSS has considerable effects on the tracking speed and steady-state oscillation of MPPT. If the PSS is too small, the tracking speed will be too slow. On the other hand, if the PSS is too large, the steady-state oscillation will be intensified.

In order to solve this problem, researchers have proposed many new MPPT algorithms that can be applied in fast varying solar irradiance conditions and that have rapid tracking speeds and low steady-state oscillation [6–27]. These methods can be divided into three

categories as follows: (1) mathematical model based MPPT techniques, (2) two-stage MPPT approaches, and (3) variable step size (VSS) MPPT methods. In the first category, Refs. [6,7] estimates the maximum power point (MPP) location according to mathematical models, Ref. [8] calculates MPP utilizing a fuzzy controller, Ref. [9] acquires MPP employing extremum seeking control (ESC), Ref. [10] obtains MPP by using sliding mode control (SMC), and Ref. [11] calculates MPP utilizing backstepping super-twisting sliding mode control (BSTSMC). These techniques can achieve highly rapid tracking speed; however, an accurate PV cell model and complex calculation are necessary. Regarding the second category, mathematical analysis or numerical methods are utilized in the first stage to move the operating point (OP) to the vicinity of real MPP; then a second stage is applied to acquire the real MPP [12–14]. For these methods, Newton–Raphson method [12], the beta method [13], and Lagrange interpolation formula [14] are employed in the first stage. In the second stage, P&O [12,13], and particle swarm optimization (PSO) method [14] are adopted. Similarly, complex calculations are needed for these methods. As for the third category, MPPT methods use the distance between the current operating point (OP) and the MPP to determine the PSS. Once OP is close to MPP, a small PSS is then applied, and vice versa. VSS MPPT algorithms include the algorithms which uses many fixed steps according to the operating points [15,16], and the adaptive variable step size algorithms [17–27]. Among these algorithms, the adaptive variable step size algorithm has received attention from many researchers due to its advantages of simple calculation, easy implementation, and easy integration with conventional methods such as P&O or IncCond. Among the adaptive variable step size algorithms proposed in the literature, the PSS is determined by the ratio of power to voltage (dP/dV) [17,19,22–24,27], the ratio of power to duty cycle (dP/dD) [18], the ratio of power to current (dP/dI) [11], the ratio of current to duty cycle (dI/dD) [21], the ratio of power to the difference between the voltage and the current ($dP/(dV-dI)$) [25], and the power variation (dP) [26]. For these methods, the above variables must be multiplied by scaling factors to obtain the PSS needed by the systems. In the literature mentioned above, most of the scaling factors used are constants. However, suppose the same scaling factor is used under all irradiance levels. In that case, the system performance will be optimal only under a specific irradiance level and will be poor under other conditions and may cause oscillation and/or slow tracking speed. Hence, in Ref. [24], ($k_1 - k_2 \cdot P$) was proposed to adjust scaling factors automatically; however, the two constants of k_1 and k_2 must still be determined in this method without ensuring the optimal values. In Ref. [26], two different scaling factors were proposed for different irradiance levels (high level and low level). Still, similarly, the system performance may be unable to be optimized under certain irradiance levels if only two scaling factors are adopted. In conclusion, the scaling factor plays a significant role in an adaptive VSS MPPT method; hence, it should be chosen carefully to enhance the MPPT performance. However, it remains a challenging task to determine an optimal scaling factor based on the operating conditions.

On the other hand, artificial neural network (ANN) has been widely applied to estimate SPGS's maximum power point [28–37]. The benefits of using ANN are that there is no requirement for knowledge on accurate mathematical models, less computational effort, and the capability of providing a compact solution for multivariable problems. ANN-based MPPT techniques vary from several aspects, including (i) controller configuration, (ii) required input signals, and (iii) output signals. In the controller configuration aspect, Refs. [28,29] uses ANN as the controller to improve the performance of the conventional PID controller; Refs. [30–37] utilizes ANN to estimate MPP. In the required input signals aspect, most of the literature uses irradiance value and panel temperature as the ANN input [30–34,37]. However, the measurement of irradiance and panel temperature requires more expensive sensors, which may increase the system cost. Additionally, the accuracy and robustness of these sensors are inferior. On the other hand, Ref. [30] uses open circuit voltage (V_{oc}) and short circuit current (I_{sc}) as the ANN input, but the regular actions need to be stopped when measuring V_{oc} and I_{sc} , which leads to power loss. Finally, Ref. [36] uses the magnitude of a power variation (dP) and the magnitude of a voltage variation (dV) as the

input. In the output signals aspect, common ANN output includes the corresponding duty cycle value of the MPP (D_{MPP}) [30], the corresponding current command value of the MPP (I_{MPP}) [31,33], the corresponding voltage command value of the MPP (V_{MPP}) [32,33,35], the power value of the maximum power point (P_{MPP}) [34,37], and the tracking direction command of the duty cycle [36]

In this study, an ANN-assisted MPPT method is proposed. The proposed method utilizes a neural network to obtain an optimal scaling factor according to current irradiance level using the measured voltage and current value of two consecutive perturbation points as the ANN's input. To the best of the authors' knowledge, the proposed ANN architecture has never been shown in the literature. Compared with the adaptive scaling factor method proposed by [32], the proposed method does not require intensive simulations to gain optimal scaling factor. It can also avoid the complicated calculation, which is required when applying state estimation methods to calculate the irradiance level. The proposed method has the advantages of easy implementation, simple calculation, and optimal performance in a fast varying solar irradiance condition. The main novelty of the proposed MPPT technique are listed below:

- An optimal scaling factor according to the operating conditions is applied in the proposed VSS IncCond MPPT technique to obtain fast tracking response and reduced steady-state oscillations
- It requires fewer voltage samples than other techniques to identify the optimal scaling factor and hence enhances the tracking ability and dynamic efficiency.
- High-cost irradiance and temperature sensors are not needed comparing with other ANN-based MPPT methods.
- The proposed method can be easily integrated into the conventional VSS IncCond MPPT method, which improves its tracking performance

To verify the proposed MPPT method's effectiveness, the proposed method is compared with several MPPT methods suitable for fast-varying environments proposed in other literature, including the VSS IncCond, α -P&O [33], and golden section [34] MPPT methods. According to the simulation and experimental results, this proposed method has the optimal tracking accuracy, and both tracking time and tracking loss are only preceded by the golden section method in the uniform insolation conditions. When applied in the varied insolation condition, the tracking time, tracking accuracy, and the overall tracking loss of the proposed method are best among all the compared methods. When utilized in the fast varying irradiation conditions, the proposed method is far superior to other methods. As a result, to conclude from its overall performance, the proposed method has great performance in different operating conditions.

2. Mathematical Modeling and Conventional Variable Step Size Incremental Conductance MPPT Algorithm

In this section, the mathematical modeling of the solar cell will be presented first. Additionally, the description of conventional VSS IncCond MPPT method and some discussions about the effect of the scaling factor on the MPPT performance will be provided.

2.1. Solar Cell Characteristics

This study uses the common single diode model to simulate the solar cell characteristics; Figure 1 shows the solar cell model used by this study; through Figure 1, the relation of output current and voltage can be expressed as below:

$$I_T = I_g(S, T) - I_s(T) \left(e^{\frac{q(R_S I_T + V_T)}{KATN}} - 1 \right) - \frac{R_S I_T + V_T}{R_P} \quad (1)$$

where q , K , T , and N are the electron charge (1.602×10^{-19} C), Boltzmann constant (1.38065×10^{-23} J/K), panel temperature in Kelvin, and the number of cells connected in series, respectively. $I_g(S, T)$ is the photoelectric current for a certain solar irradiance level

S (W/m^2) and panel temperature T , and $I_s(T)$ is the reverse saturation current under a specific panel temperature. A , R_S , and R_P are the diode ideality factor, equivalent series resistance, and equivalent shunt resistances, respectively. $I_g(S, T)$ and $I_s(T)$ can further be expressed by

$$I_g(S, T) = \frac{S}{1000} \times (I_{SC} + \alpha_{I_{SC}} \cdot (T - T_0)) \tag{2}$$

$$I_s(T) = C_0 \cdot T^3 \cdot e^{(-\frac{E_g}{kT})} \tag{3}$$

where $\alpha_{I_{SC}}$ is the temperature coefficient of I_{SC} , I_{SC} stands for the short-circuit current of the PV module, T_0 is cell temperature under standard test condition (STC), C_0 is the temperature coefficient, E_g is the material bandgap. After formulating the relation of the solar panel output voltage and current, the output power can be acquired by multiplying the output voltage by the current. Figure 2 illustrates the characteristic curves of power versus voltage and their absolute slope values under different irradiance levels of the solar panels used in this study. In Figure 2, the slope of the P-V curve is defined as the derivative of power to voltage (dP/dV).

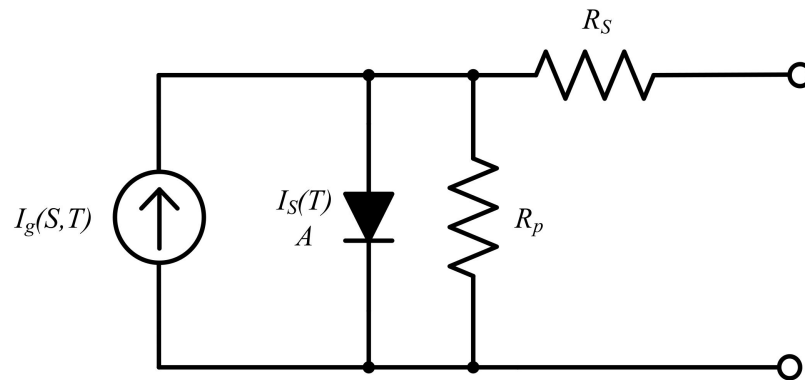


Figure 1. Single diode equivalent circuit model of the solar cell.

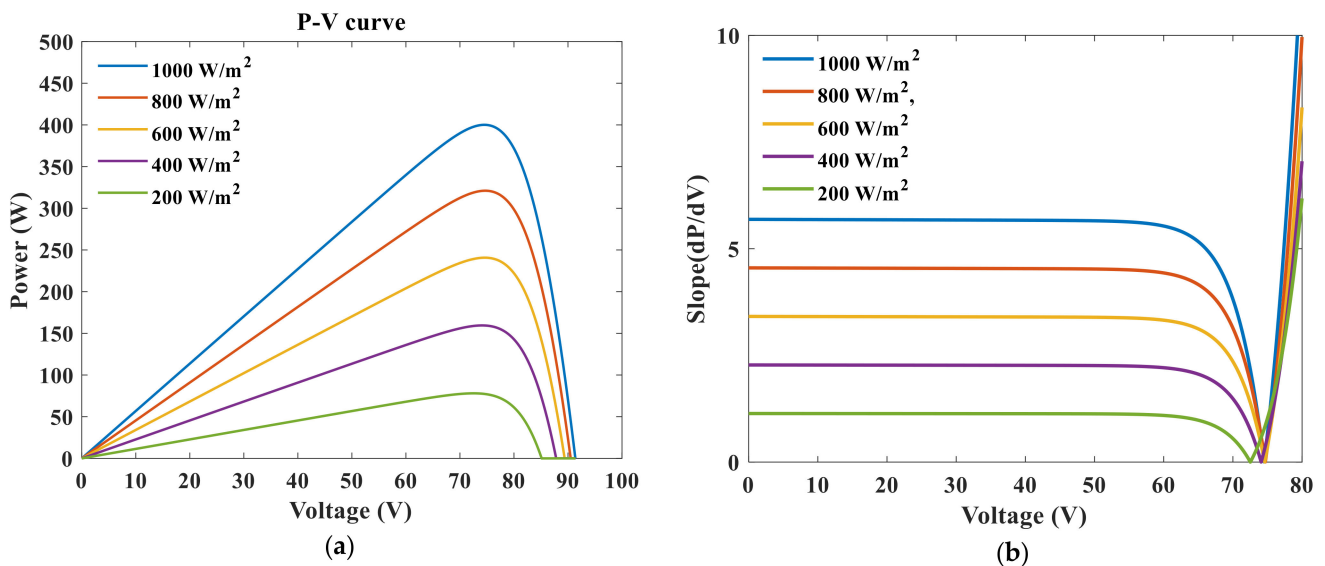


Figure 2. Characteristic curves of the utilized JAM5(L)72-200/SI solar cell (a) P-V curves (b) absolute slope of P-V curves.

2.2. Variable Step Size Incremental Conductance MPPT Algorithm

Conventional IncCond MPPT method uses fixed PSS to track the MPP; however, although larger PSS acquires faster tracking speed, the oscillation generated around MPP decreases its tracking accuracy and increases the power loss. On the contrary, although

smaller PSS can achieve higher tracking accuracy and lower power loss, it leads to slower tracking speed. Therefore, how to make a tradeoff between tracking speed, tracking accuracy, and power loss is an essential problem in the conventional fixed PSS IncCond MPPT method. Hence, the literature [9] proposed a VSS IncCond MPPT method to alleviate this problem. In the VSS IncCond MPPT method, its PSS can be calculated through Equation (4). It is generated by multiplying a scaling factor by a P–V curve slope value (dP/dV) of its operating point (OP). As Figure 2 shows, the P–V curve slope value is larger when OP is far from MPP; thus, a larger PSS can be taken to approach MPP. When OP approaches MPP, the slope value becomes smaller. Moreover, when OP equals to MPP, the slope value becomes 0. In this way, the steady-state oscillation can be minimized, thus achieving the purpose of solving the tradeoff problem between tracking speed and tracking accuracy.

$$V_{(n+1)} = V_{(n)} \pm M \cdot \left| \frac{dP}{dV} \right| \quad (4)$$

In Equation (4), scaling factor M is usually a fixed value, and it can be further designed in accordance with Equation (5). In Equation (5), $|dP/dV| \Delta V_{\max}$ represents the maximum slope when PSS is ΔV_{\max} under STC. However, as Figure 2 shows, the maximums of P–V curve slopes are different under various irradiance levels; therefore, providing that in order to reach the same ΔV_{\max} , the required optimal M values vary under different irradiance level as well. When under high irradiance levels, a smaller M should be selected due to the higher slope; when under low irradiance levels, a larger M should be picked. In other words, a large value of M is beneficial for the tracking speed; however, it will result in substantial oscillations around the MPP. In contrast, a small value of M can cause the MPP tracking speed becomes slow. For different conditions, the required scaling factor is different, which limits the universality of the method.

$$N < \Delta V_{\max} / \left| \frac{dP}{dV} \right|_{\Delta V_{\max}} \quad (5)$$

Therefore, to ensure the VSS IncCond MPPT method has the optimal tracking speed, tracking accuracy, and power loss under each irradiance levels, this study proposed an improved VSS IncCond MPPT method to select the most appropriate scaling factor for the current operating environments. This study uses ANN to conduct the calculation of the optimal scaling factor; the design and implementation of ANN will be explained in the next section.

3. Description of the Proposed Method

The skill proposed by this study firstly uses ANN to estimate the optimal scaling factor (OSF) that should be used in current irradiance levels, then using VSS IncCond MPPT method to track the maximum power point. This section will first introduce the OSF estimation method implemented by ANN and the way to conduct VSS IncCond MPPT by using the estimated OSF.

3.1. Neural Network Design and Implementation

Neural network builds mathematical models by imitating the data processing of biological neural network, using a neural network can simulate the system behaviors, which are complicated and not easy to model, without the premise of precise mathematical models; a typical artificial neural network mathematical model is composed of several neurons, as Figure 3 illustrates. The relation between the neuron's input and output is shown in Equation (6); it is an output gained by multiplying the input by weight and sums then converts through an activation function. The so-called neural network training means to meet the expected output by modifying weights and bias. During training, ANN usually generates initial weight values between +1 and –1 randomly. The weights function is similar to the effect of synapsis; if the weights are larger, the connected neurons will be

activated easily, then the impact on the network becomes more evident; on the contrary, there will be a smaller impact on the neural network when the weights are smaller.

$$Y = \sum W_i X_i - b \tag{6}$$

where X , W and b are input, weight and Bias, Σ is summation, and f is activation function, its objective is to map the Σ value to the corresponding output, Y is output, the users' expected results, i should be in the range of $[1, n]$, where n is the size of input data.

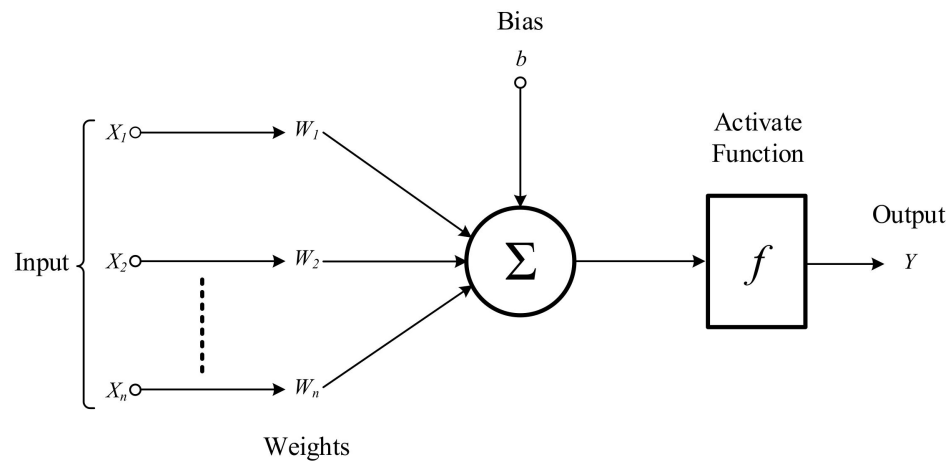


Figure 3. Concept of neurons.

This study uses a back-propagation neural network; its architecture can be divided into Input Layer, Hidden Layer, and Output Layer. Input Layer is composed of single or multiple neurons; the number of input neurons is related to the problems to be solved. Hidden Layer is a single or multiple layer neurons between Input Layer and Output Layer; its purpose is to represent the nonlinear relation between input and output. Hidden Layer's configuration should be decided based on the complexity of the problems; however, there is currently no standard method to determine the configuration of Hidden Layer; a better setting value is usually acquired through multiple tests. Output Layer is the ANN's output; likewise, the number of output neurons is related to the problems.

Figure 4 shows a schematic diagram of the proposed OSF estimation neural network architecture, and is explained as follows. This study designed a four-layered neural network architecture, which includes one Input Layer, two Hidden Layers, and one Output Layer, respectively. The neural network input parameters used by this study are two solar cell operating voltages $V(t)$, $V(t) + \Delta V$, and the power change ΔP measured by these two consecutive perturbations; ΔP is defined as $P(V(t) + \Delta V) - P(V(t))$; the output parameter is the OSF; the two Hidden Layers contains 10 neurons respectively, and the activation function is Tansig, as shown in Equation (7). Levenberg–Marquardt method is used as the training method in this study.

$$y(n) = \frac{e^n - e^{-n}}{e^n + e^{-n}} = \text{Tansig}(n) \tag{7}$$

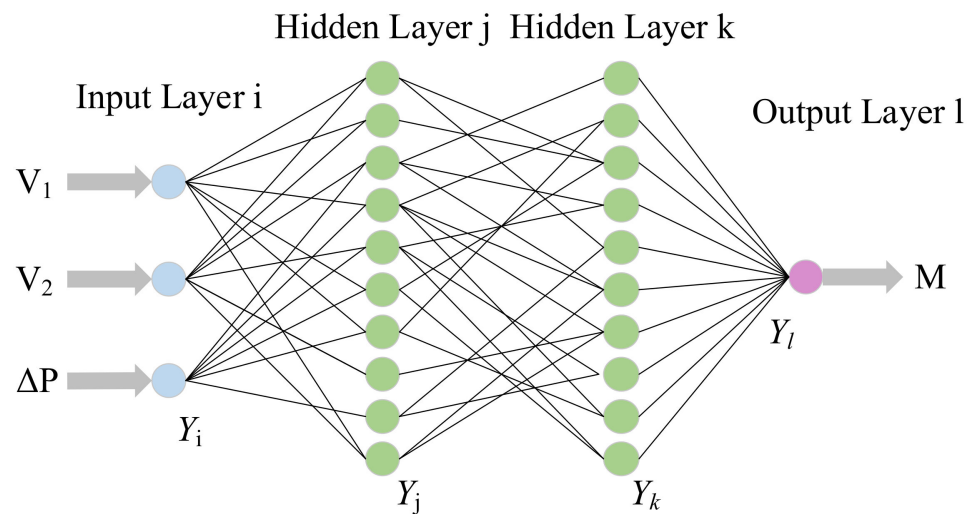


Figure 4. ANN architecture for estimating OSF value proposed in this study.

The accuracy of the neural network is directly related to the completeness of the training set. In the following, the method of generating the training set of the proposed neural network will be described in detail. First, set the irradiance level as 100 W/m^2 ; then initialize the voltage as 0 V ; after that, in every interval of ΔV , the voltage values of the previous and current points, as well as the power difference between these two points, need to be calculated as the neural network input; Matlab is then used to conduct the simulation of IncCond method to find out the OSF value under this irradiance level, and the obtained OSF is then utilized as the output parameter of the ANN. When the operating voltage reaches the VOC under certain irradiance level, adds 100 W/m^2 to the irradiance level and sets the voltage to the initial value, 0 V . This procedure should be conducted repeatedly until the irradiance level reaches 1000 W/m^2 . This study uses 0.1 V for ΔV ; therefore, a total of 16,691 training data can be obtained. Additionally, this study acquires a total of 2630 verification data under the simulated irradiance level of 210 W/m^2 , 510 W/m^2 , and 810 W/m^2 .

3.2. Flow Chart of Proposed ANN-Assisted VSS IncCond MPPT Algorithm

The conventional VSS IncCond MPPT algorithm has advantages in high tracking speed, high accuracy, low tracking loss, etc. However, the fixed scaling factor makes its performance significantly decrease when irradiance level changes; therefore, this study proposed an ANN-assisted VSS IncCond MPPT algorithm. Figure 5 is the flow chart of the proposed method, and the dashed line part in this figure is the conventional VSS IncCond MPPT method. As Figure 5 implies, the proposed method will first generate the two OPs— $V(t)$, and $V(t) + \Delta V$, then record its voltage and current information; next, input $V(t)$, $V(t) + \Delta V$, and the power change ΔP to the trained ANN to obtain the OSF of current irradiance level; then conduct the VSS IncCond MPPT method by using this scaling factor value. When the irradiance level changes, the system should still operate the two OPs to estimate the new OSF value. This study selects the OSF based on the trained ANN, which can ease the scaling factors tradeoff problem. The proposed method has advantages in high tracking speed, non-steady-state concussions, etc. under any circumstances.

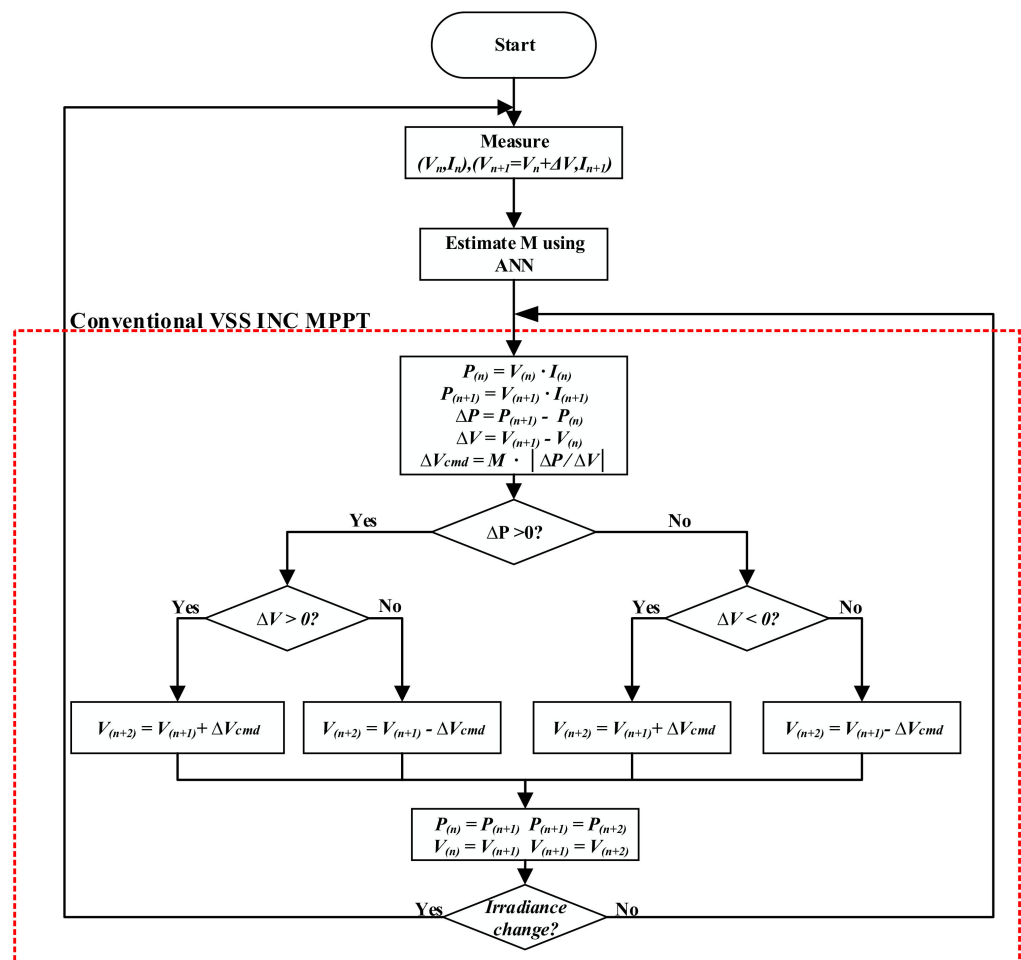


Figure 5. Flow chart of the proposed ANN-assisted VSS IncCond MPPT Algorithm.

4. Simulation and Experimental Results

4.1. Performance Index (PI)

To fairly evaluate and compare the test results of different tracking methods, a performance index (PI) is defined in this study. Figure 6 is a typical MPP tracking response. The criterion defined for each measured item illustrated in Figure 6 is described as follows: (1) Tracking time (Tr): the time required for the tracking power increases to 95% of maximum power; (2) Steady-state tracking accuracy (Acc): dividing the Steady-state average power by the specific MPP; (3) Tracking energy loss (Loss): the shaded area as shown in Figure 6. It records the power for a pre-set duration and takes the absolute value of the MPP value minus the tracked power value.

Figure 7 shows the block diagram of the proposed MPPT system; this study uses MATLAB/SIMULINK to establish a simulation platform. To verify the superiority of the proposed method, this method compared the tracking performance with four methods proposed in the literature, including conventional perturb and observe (P&O) method, conventional VSS IncCond approach [18], alpha-perturb and observe (α -P&O) techniques [38], and golden section (GS) method [39]. In P&O, a small voltage perturbation changes the solar panel’s power. Providing that the power variation is positive, voltage perturbation remains in the same track. However, if power difference is negative, the perturbation direction will be reversed. The concepts of α -P&O method and the conventional P&O technique are similar, which continuously perturbs around the MPP. Unlike conventional P&O, the perturbation step of α -P&O gradually decreases until it reaches the minimum step allowed by the system. The golden section method converges to the MPP by interval shrinking. In the beginning, two points are chosen from the search space with known

boundaries, and the two points will be assessed. Then, a new point is generated accordingly. At a given iteration, the algorithm has a new narrowed interval bounded by the new point as well as one of the initial points based on the evaluation results. The algorithm keeps iterating (interval shrinking) until the interval becomes small enough. The parameters used by the simulation are shown in Tables 1 and 2; the simulation results are shown in Figure 8 and Table 3. Figure 8 is the tracking waveforms of each compared method in a total simulation time of 1 s under the irradiance level of 500 W/m^2 ; Table 3 lists the tracking performances of each different method in a total simulation time of 1 s under the irradiance level of $100\text{--}1000 \text{ W/m}^2$ (100 W/m^2 in each interval, ten kinds in total). In Table 3, the light red parts indicate the methods with the best PI under a single test condition; the methods with the worst PI are marked in light green. As Figure 8 and Table 3 show, the P&O method uses a larger PSS to attain a shorter dynamic tracking time, which results in a steady-state oscillation, making its average tracking accuracy below 98%; tracking loss above 30 W. As the conventional VSS IncCond method uses a constant M value that is suitable only to the irradiance level of 1000 W/m^2 , it has a slower tracking speed under other irradiance levels. Moreover, the tracking accuracy is even below 60% under 100 W/m^2 because it did not reach a steady state at the end of the test. The other three methods' performances are close to each other on the three performance indexes. Moreover, GS has the best performance in the average tracking time; the proposed method and the α -P&O are the second, but the differences are not evident. The proposed method has the best performance with 99.91% in the average tracking accuracy; followed by 99.26% in GS and 98.97% in α -P&O. Lastly, as GS can reach steady-state more rapidly, it has the best performance with 14.45 W in its average tracking loss, followed by 21.97 W in the proposed method and 27.96 W in α -P&O. Regarding to Table 3, the proposed method has the best performance of the tracking accuracy under each irradiance level. As for tracking speed, the proposed method and GS lead one another alternately. Moreover, the proposed method is inferior to GS in terms of tracking loss.

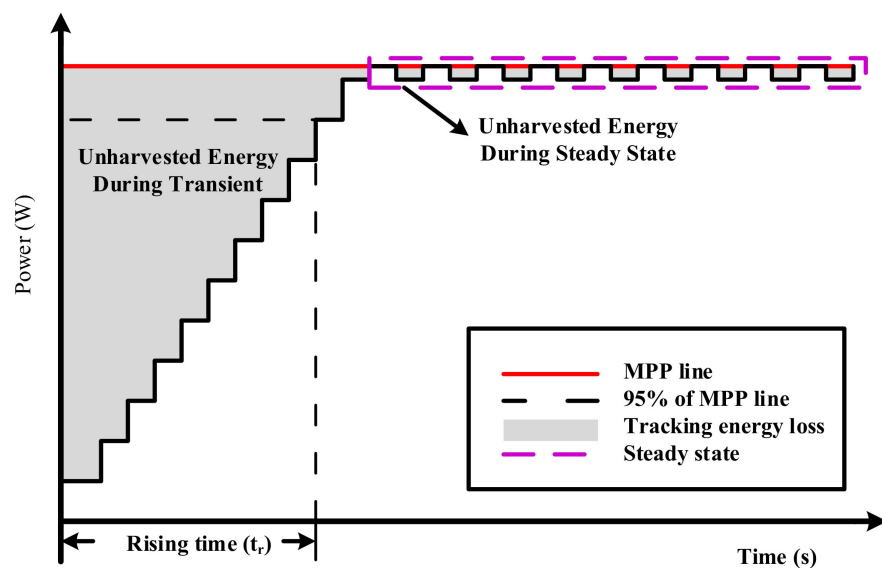


Figure 6. Tracking response of the MPPT operation.

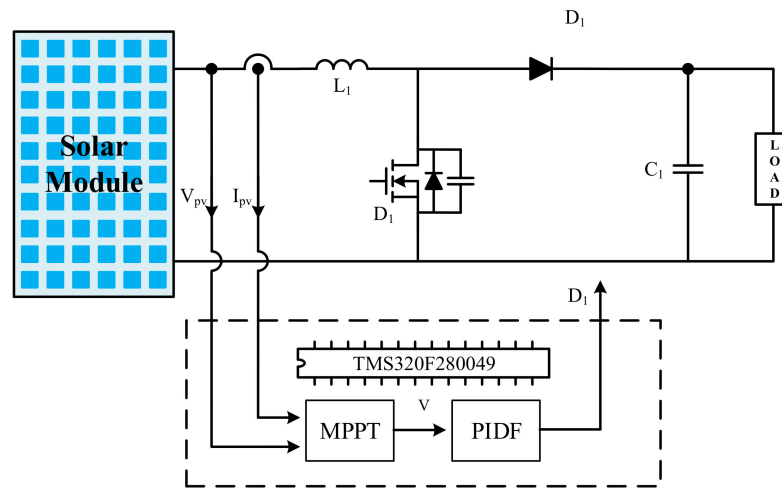


Figure 7. Block diagram of the proposed MPPT system.

Table 1. Parameters of the utilized boost converter.

Parameters	Boost Converter
Switching frequency	50 kHz
Sampling time	0.1 s
Input inductor	1.08 mH
Switches	IPP65R110CFDA
Filter capacitor	100 μ F

Table 2. Specification of the utilized PV Module.

Parameters	Value
Maximum PV Power	400 W
Voltage at MPP	74.22 V
Current at MPP	5.39 A
Open circuit voltage, V_{oc}	91.38 V
Short circuit current, I_{sc}	5.69 A

Note: Irradiance 1000 W/m² and module temperature 25 °C.

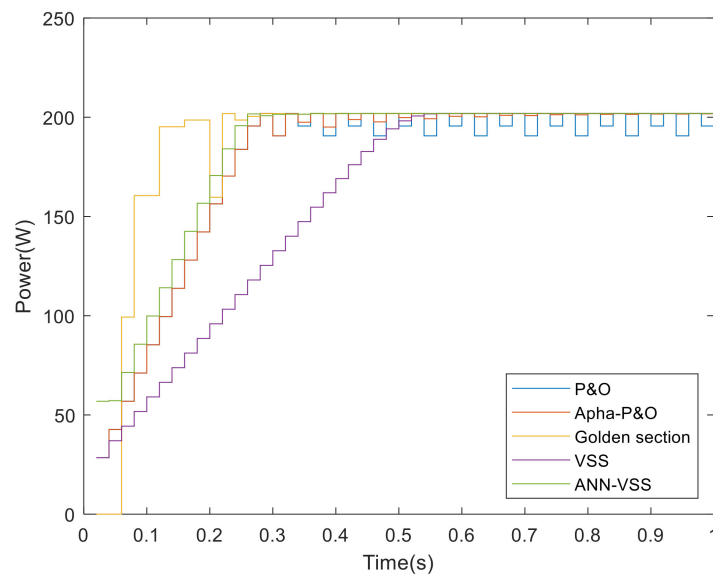


Figure 8. Simulated tracking waveforms of five compared MPPT methods (500 W/m²).

Table 3. Simulated results of five compared MPPT methods under uniform insolation condition.

Irradiance		P&O	α -P&O	GS	VSS	Proposed
100	Tr (s)	0.26	0.26	0.26	>1 (1.96)	0.26
	Acc (%)	95.51	98.52	95.51	59.04 (99.33)	99.92
	Loss (Ws)	4.9	4.07	2.35	22.18	2.99
200	Tr (s)	0.28	0.28	0.28	>1 (1.06)	0.28
	Acc (%)	97.95	99.32	99.8	92.13 (99.18)	99.84
	loss (Ws)	9.29	8.49	4.63	33.96	6.69
300	Tr (s)	0.28	0.28	0.26	0.78	0.28
	Acc (%)	95.61	98.43	99.9	99.14	99.9
	loss (Ws)	16.68	14.23	7.17	37.52	0.69
400	Tr (s)	0.28	0.28	0.24	0.62	0.28
	Acc (%)	97.23	99.08	99.84	99.63	99.91
	loss (Ws)	21.12	18.94	9.93	40.1	14.89
500	Tr (s)	0.28	0.28	0.3	0.48	0.28
	Acc (%)	97.88	99.76	97.88	99.43	99.97
	loss (W)	26.17	23.85	13.71	42.38	19.24
600	Tr (s)	0.28	0.28	0.28	0.44	0.28
	Acc (%)	98.1	99.44	99.93	99.8	99.86
	loss (Ws)	31.71	29.29	15.77	44.47	23.72
700	Tr (s)	0.3	0.3	0.3	0.4	0.3
	Acc (%)	98.12	99.26	99.9	99.83	99.84
	loss (Ws)	37.67	35.22	18.57	46.44	28.28
800	Tr (s)	0.3	0.3	0.3	0.34	0.3
	Acc (%)	97.99	98.88	99.93	99.83	99.95
	loss (Ws)	43.97	41.85	21.28	48.32	32.96
900	Tr (s)	0.3	0.3	0.3	0.32	0.3
	Acc (%)	95.33	98.43	99.94	99.91	99.94
	loss (Ws)	57.39	49.01	24.11	50.14	37.71
1000	Tr (s)	0.3	0.3	0.24	0.3	0.3
	Acc (%)	96.10	98.6	99.94	99.89	99.94
	loss (Ws)	62.22	54.65	27.02	53.34	42.53
Average	Tr (s)	0.29	0.29	0.28	0.46	0.29
	Acc (%)	97.08	98.97	99.26	94.86	99.91
	loss (Ws)	31.11	27.96	14.45	41.89	21.97

Note: the light red parts indicate the methods with the best PI under a single test condition; the methods with the worst PI are marked in light green.

In this study, the optimal scaling factors for different irradiance level are obtained via intensive simulations. To fairly evaluate and compare the acquired results of different scaling factor values, tracking energy loss (E_{loss}) is utilized as performance index in this study. Tracking energy loss is adopted because it can simultaneously take the tracking time and steady-state tracking accuracy into account. Figure 2 shows a typical tracking response of one MPP tracking curve under certain irradiance level and panel temperature. The tracking energy loss in this study is defined as the area between the exact MPP and the power tracking curve within a certain time interval, as shown in the shaded part of Figure 2. To take both transient and steady-state responses into account, the total simulation time was set as 10 s. This study simulated 10 possible operating conditions (10 irradiance levels

(100–1000 W/m²) with the interval 100 W/m² under constant panel temperature (25 °C)). In this study, the range of tested scaling factor is 0.1–10.0. With the interval of 0.01, there are 990 possible scaling factor values and the scaling factor with the best tracking energy loss under 10 different operating conditions will be recorded. The parameters used for the simulations are as detailed in Tables 1 and 2, the obtained optimal scaling factor values are listed in Table 3.

Figure 8 and Table 3 summarize the test results under the uniform insolation condition; however, a typical SPGS is often subjected to irradiance change. Therefore, this study focuses on the irradiance change in Figure 9 next to conduct MPP tracking with these five different MPPT methods mentioned previously and illustrate the acquired tracking waveforms into the same figure for comparison. The calculated tracking time, tracking accuracy, and tracking loss of each method in each section are listed in Table 4. In Figure 9, the irradiance change is listed as following: 515 W/m² from 0 to 1 s; 1000 W/m² from 1 to 2 s; 325 W/m² from 2 to 3 s. As Figure 9 and Table 4 show, the P&O method’s steady-state oscillation makes it perform the worst in tracking accuracy and tracking loss. Similarly, as VSS does not utilize the optimal scaling factor value for each irradiance level, a longer tracking time is observed in the first step, which results in higher tracking loss.

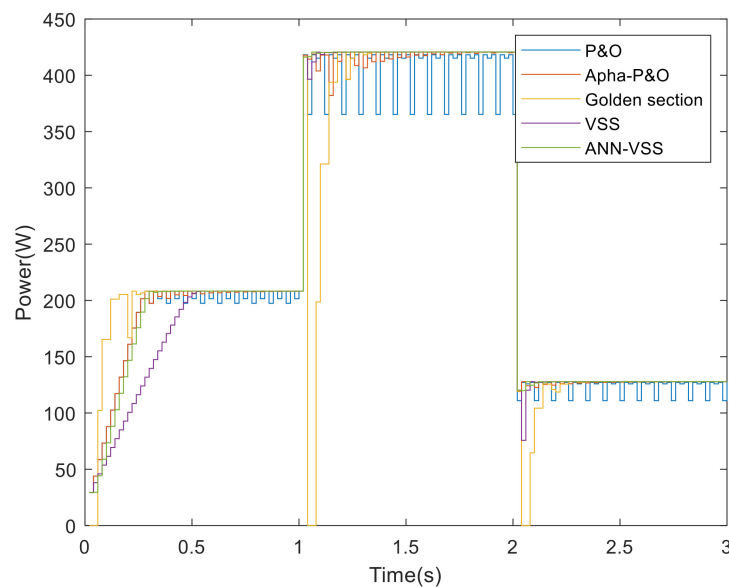


Figure 9. Simulated tracking waveforms of five compared MPPT methods under varying irradiation condition.

Table 4. Simulated results of five compared MPPT methods under varying irradiation condition.

Irradiance		P&O	α-P&O	Golden	VSS	Proposed
515	Tr (s)	0.28	0.28	0.29	0.48	0.28
	Acc (%)	98.86	99.5	99.71	99.69	99.87
1000	Tr (s)	0.72	0.72	0.23	0.06	0.04
	Acc (%)	95.97	99.13	97.45	99.8	99.94
325	Tr (s)	0.55	0.55	0.22	0.04	0.01
	Acc (%)	99.17	99.59	99.8	99.9	99.91
Average Tr(s)		0.52	0.52	0.25	0.19	0.11
Average Acc(%)		98.00	99.41	98.99	99.80	99.91
Total Loss(Ws)		49.06	28.94	48.65	44.89	27.97

Note: the light red parts indicate the methods with the best PI under a single test condition; the methods with the worst PI are marked in light green.

It is notable that when the irradiance level varies, α -P&O needs to adjust the PSS back to the maximum, and GS needs to restart tracking procedures. These facts result in slower tracking speed and higher tracking loss. Particularly, as the variation of the voltage command is large when GS restarts tracking process, the average tracking loss increases significantly, only preceded by P&O. As Table 4 indicates, in comparison with P&O, the proposed method improves tracking speed by 78.84%, tracking accuracy by 1.94%, and tracking loss by 42.98% on average under the tested scenario. In comparison with α -P&O; it improves the tracking speed by 78.84%, tracking accuracy by 0.5%, and tracking loss by 3.35%. In contrast with GS, it improves the tracking speed by 56%, tracking accuracy by 0.92%, and tracking loss by 42.5% on average. In comparison with VSS, it improves tracking speed by 42.1%, tracking accuracy by 0.11%, and tracking loss by 37.69% on average.

Lastly, this study focuses on the tracking performance when there is fast change in irradiation. Figure 10 shows the simulated results of the proposed method, and Table 5 indicates the total loss. In Figure 10, the simulated scenario are listed as following: the irradiance level is 300 W/m^2 from 0 to 3 s; the irradiance level increases by 100 W/m^2 every 1 s from 3 to 9 s until it reaches 1000 W/m^2 ; the irradiance level is fixed as 1000 W/m^2 from 9 to 19 s; the irradiance level decreases by 100 W/m^2 every 1 s to 300 W/m^2 from 19 to 25 s; the irradiance is set as 300 W/m^2 from 25 to 35 s; this is the testing condition with the fastest irradiance change in EN 50530:2010 standard [35]. As Table 5 shows, the steady-state oscillation of P&O makes its tracking loss greater than 331 W as the worst of all; GS needs to restart tracking procedure due to irradiance change; therefore, its tracking loss reached 247 W. These two values are much higher than those of the other three compared methods. As Table 5 implies, in the tracking loss aspect, compared with P&O, α -P&O, GS, and VSS, the proposed method can improve by 95.46%, 41.73%, 93.92%, and 67.56%, respectively.

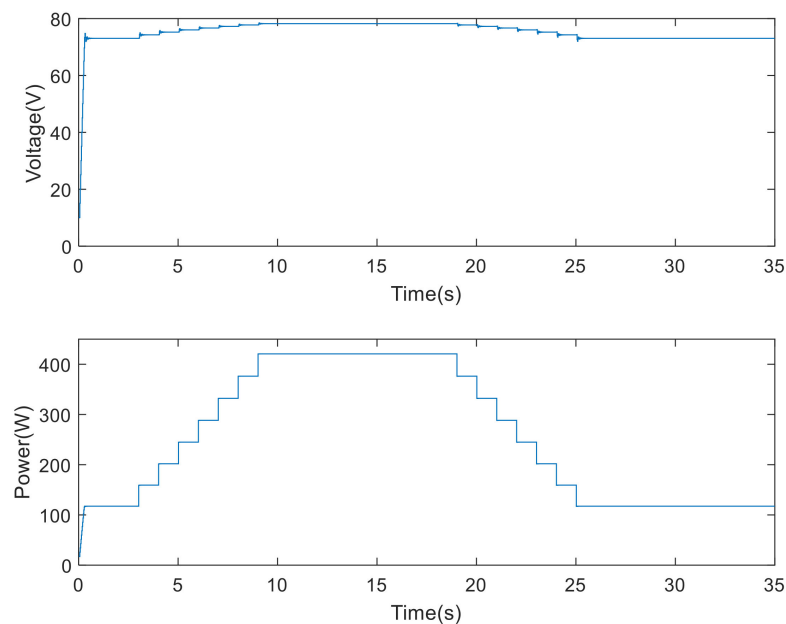


Figure 10. Tracking waveforms of the proposed method under EN50530 test condition.

Table 5. Simulated results of five compared MPPT methods under varying irradiation conditions.

	P&O	α -P&O	Golden	VSS	Proposed
Total loss (Ws)	331.34	25.78	247.37	46.31	15.02

Note: the light red parts indicate the methods with the best PI under a single test condition; the methods with the worst PI are marked in light green.

4.2. Experimental Result

To further verify the correctness of the proposed method, this study also carries out experiments on these five MPPT method mentioned above. In this paper, a 400 W prototyping circuit is implemented from which experiments are carried out accordingly. Figure 11 shows a photo of the proposed system. In Figure 11, a low-cost DSP TMS320F280049 from Texas Instruments (Dallas, TX, USA). is used to realize the MPPT algorithms mentioned above.

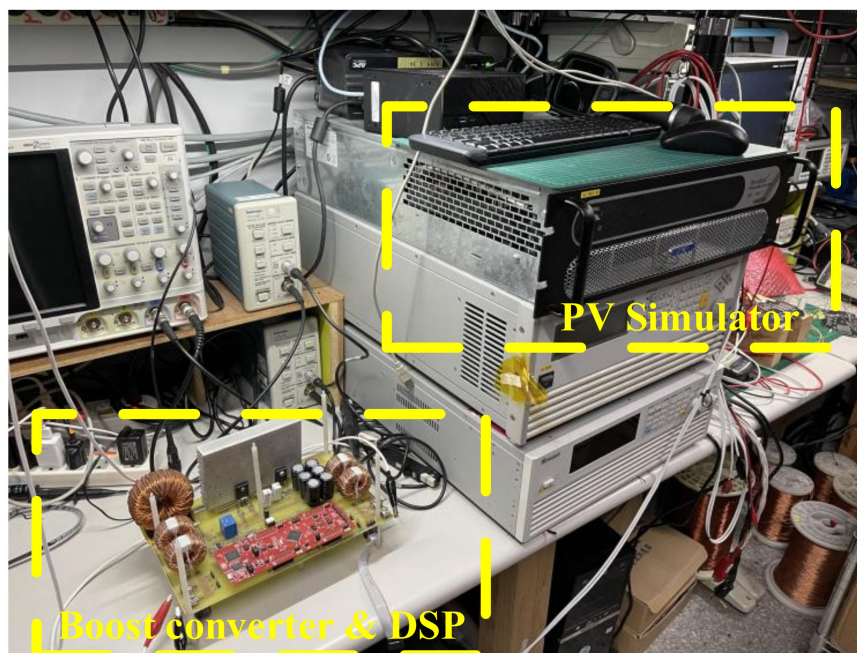


Figure 11. Experimental setup and the testing environment.

The experiments are performed with an AMETEK TerraSAS DCS80-15 solar array simulator (San Diego, CA, USA) in SAS mode as a power source. The parameter used in the experiment is identical to the ones used in the simulation. Figure 12 and Table 6 illustrates the tracking performance of these five MPPT methods under the uniform insolation condition; Figure 13 and Table 7 shows the tracking performance of these five MPPT methods under varying irradiation condition; Figure 14 shows the tracking waveform of the proposed method under the EN50530 testing condition, and Table 8 summarizes the tracking performance of each method in the EN50530 testing condition. As Figures 12–14 show, the obtained experimental results is similar to the ones acquired from the simulation, proving the accuracy of the simulated results. As Table 6 shows, similarly, P&O possesses the worst average tracking accuracy and tracking loss under the uniform insolation conditions. Since conventional VSS IncCond MPPT method does not adopt OSF according to irradiance levels, it has a slow tracking speed and poor tracking accuracy in the low irradiance levels. The other three methods' performances are close to each other on the three performance indexes; likewise, GS has the best performances in terms of average tracking time and average tracking loss; the proposed method outperforms others in the average tracking accuracy aspect. As Table 7 indicates, in the tested irradiance change environments, in comparison with P&O; the proposed method improves tracking speed by 78.84%, tracking accuracy by 1.58%, and tracking loss by 45.59% on average; compared with α -P&O; it enhances the tracking speed by 78.84%, tracking accuracy by 0.9%, and tracking loss by 6.67% on average; in contrast with GS, it improves the tracking speed by 56%, tracking accuracy by 0.53%, and tracking loss by 45.3% on average; in comparison with VSS, it enhances tracking speed by 42.1%, tracking accuracy by 0.01%, and tracking loss by 34.49% on average. As Figure 8 illustrates, in the tracking loss aspect under the EN50530 testing

condition, compared with P&O, α -P&O, GS, and VSS, the proposed method can improve by 95.58%, 42.51%, 93.66%, and 66.14%, respectively.

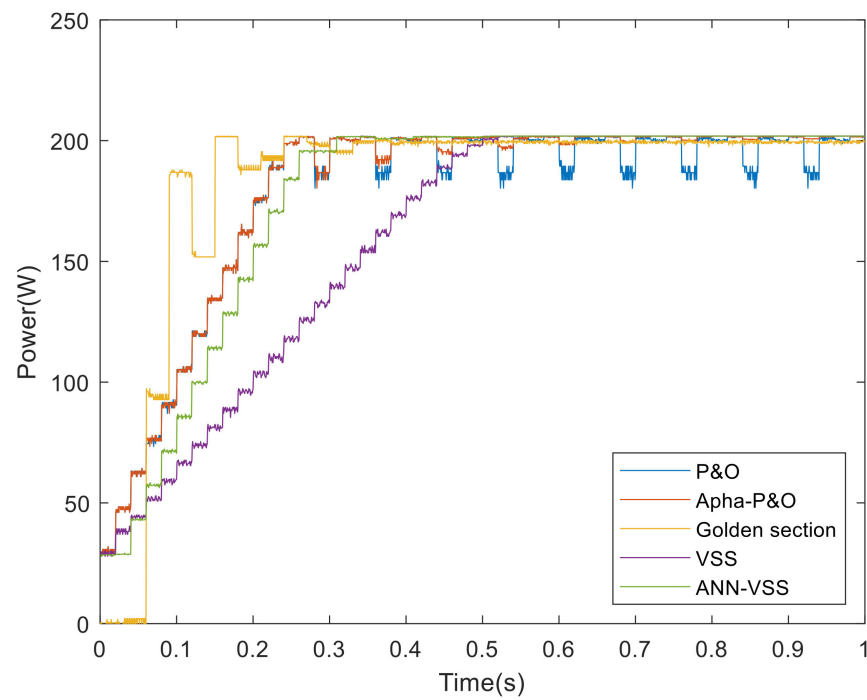


Figure 12. Experimental tracking waveforms of five compared MPPT methods (500 W/m^2).

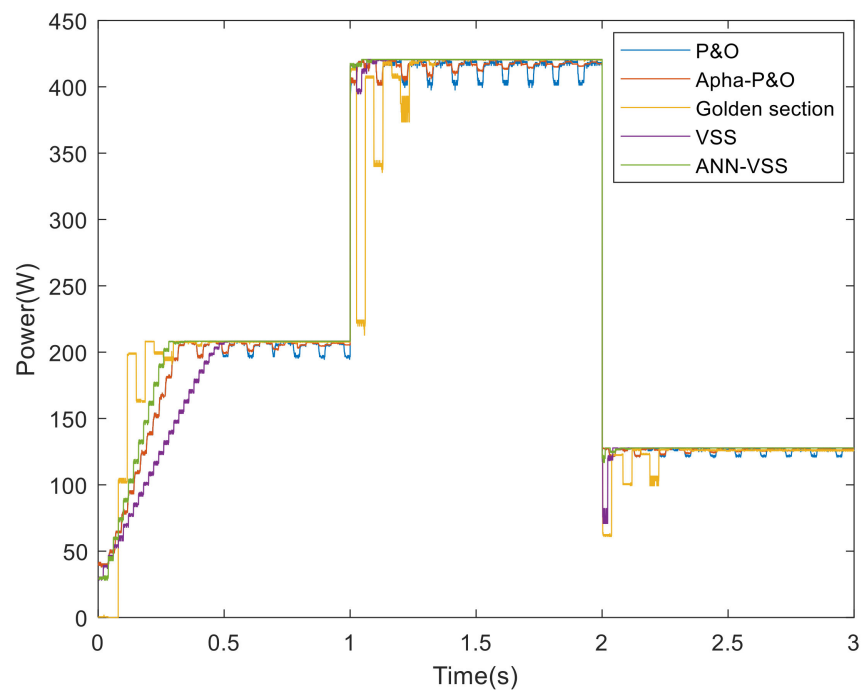


Figure 13. Experimental tracking waveforms of five compared MPPT methods under varying irradiation condition.

Table 6. Experimental results of five compared MPPT methods under uniform insolation condition.

Irradiance		P&O	α -P&O	GS	VSS	Proposed
100	Tr (s)	0.26	0.26	0.27	>1 (2.13)	0.26
	Acc (%)	96.41	97.57	95.98	58.66 (96.89)	97.66
	Loss (Ws)	4.84	3.98	2.27	20.66	2.79
200	Tr (s)	0.29	0.29	0.28	>1 (1.18)	0.29
	Acc (%)	96.72	97.03	97.57	91.67 (97.15)	97.60
	loss (Ws)	8.45	7.81	4.59	32.40	6.37
300	Tr (s)	0.28	0.28	0.26	0.74	0.28
	Acc (%)	95.43	96.62	97.21	97.00	97.38
	loss (Ws)	15.47	13.12	6.64	34.22	9.28
400	Tr (s)	0.28	0.28	0.24	0.62	0.28
	Acc (%)	96.40	98.60	97.16	98.76	99.14
	Loss (Ws)	19.72	17.57	9.55	38.86	14.50
500	Tr (s)	0.26	0.26	0.3	0.46	0.26
	Acc (%)	97.74	99.5	98.7	99.7	99.7
	loss (Ws)	25.01	22.86	12.88	42.37	18.67
600	Tr (s)	0.27	0.27	0.27	0.42	0.27
	Acc (%)	96.88	98.42	97.66	98.93	99.37
	Loss (Ws)	31.00	28.66	14.41	44.03	22.38
700	Tr (s)	0.29	0.29	0.31	0.40	0.29
	Acc (%)	97.03	97.83	98.92	99.18	99.21
	loss (Ws)	35.26	33.10	17.69	45.04	27.14
800	Tr (s)	0.30	0.30	0.31	0.33	0.30
	Acc (%)	97.22	97.68	98.10	98.35	99.30
	loss (Ws)	40.42	41.95	20.42	47.13	31.02
900	Tr (s)	0.31	0.31	0.30	0.33	0.31
	Acc (%)	95.91	97.25	98.60	99.06	99.41
	loss (Ws)	53.95	45.32	22.37	49.86	36.80
1000	Tr (s)	0.31	0.31	0.23	0.31	0.31
	Acc (%)	95.86	98.44	98.79	99.26	99.48
	Loss (Ws)	57.75	54.29	24.72	49.66	39.62

Note: the light red parts indicate the methods with the best PI under a single test condition; the methods with the worst PI are marked in light green.

Table 7. Experimental results of five compared MPPT methods under varying irradiation condition.

Irradiance		P&O	α -P&O	Golden	VSS	Proposed
515	Tr (s)	0.28	0.28	0.29	0.48	0.28
	Acc (%)	98.16	98.82	99.7	99.95	99.95
1000	Tr (s)	0.73	0.73	0.23	0.06	0.04
	Acc	98.72	99.22	99.90	99.97	99.98
325	Tr (s)	0.55	0.55	0.22	0.04	0.01
	Acc	98.41	99.07	99.44	99.97	99.97
Average Tr(s)		0.52	0.52	0.25	0.19	0.11
Average Acc(%)		98.41	99.07	99.44	99.96	99.97

Note: the light red parts indicate the methods with the best PI under a single test condition; the methods with the worst PI are marked in light green.

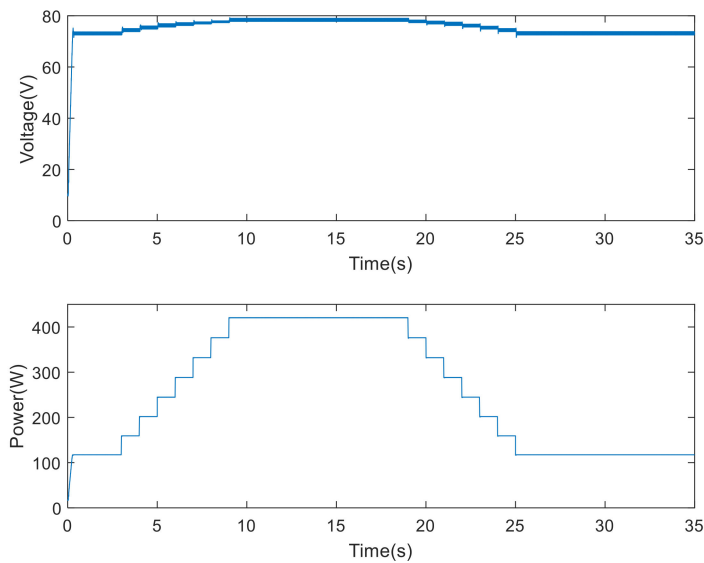


Figure 14. Experimental tracking waveforms of the proposed method under EN50530 test condition.

Table 8. Experimental results of five compared MPPT methods under EN50530 test condition.

	P&O	α -P&O	Golden	VSS	Proposed
Total loss (Ws)	376.45	28.93	262.65	49.12	16.63

Note: the light red parts indicate the methods with the best PI under a single test condition; the methods with the worst PI are marked in light green.

4.3. Discussion

Table 9 shows the average performance indices rankings of the simulation and experimental data of the five methods compared in this study under the three test scenarios. From Table 9, it can be observed that except for the ranking of the tracking accuracy of the GS method drops slightly, which is because the simulation platform adopts the floating point format while the experimental platform adopts the fixed point format, the rankings of the data acquired in the simulation and experiment of the other methods are the same on the performance indices. From the comprehensive ranking of the data in Table 9, it can be known that for uniform insolation condition, since the GS method adopts the segmented search method, it can rapidly track to the vicinity of the MPP with larger PSS. Therefore, its tracking speed and tracking loss are the best among the five methods. In contrast, conventional VSS IncCond MPPT ranks last on all of the performance indices since it cannot adopt the optimal scaling factor according to the current irradiance level, leading to a long tracking time under low irradiance circumstances. On the other hand, the method proposed in this study ranks first in tracking accuracy and ranks second in both tracking speed and tracking loss. Therefore, the GS method and the proposed method can be regarded as the most applicable of the five compared methods under uniform insolation conditions. On the contrary, conventional VSS IncCond MPPT is less applicable among the five methods. In terms of the varying irradiation condition and EN50530 test condition, since GS must restart the tracking mechanism when the irradiance varies, its tracking accuracy and tracking loss become worse; also, this phenomenon becomes more obvious when the irradiance varies more frequently. On the other hand, the conventional P&O method has the worst performance in tracking accuracy and tracking loss among the five methods since it adopts larger PSS, which leads to an obvious steady state oscillation phenomenon. Relatively, the proposed method ranks first in each performance index since it can effectively converge to MPP due to the VSS method. Additionally, it employs ANN to calculate the optimal scaling factor according to the irradiance level. In summary, the proposed method can be regarded as the most suitable method among the five methods under the varying irradiance

circumstances. On the contrary, the GS and conventional P&O methods are less suitable among the five methods.

Table 9. Rank of the performance indices of the simulated and experimental results for the five compared methods.

Insolation Condition		Simulated Results (Rank)					Experimental Results (Rank)				
		P&O	α -P&O	Golden	VSS	Proposed	P&O	α -P&O	Golden	VSS	Proposed
Uniform	Tr	2	2	1	5	2	2	2	1	5	2
	Acc	4	3	2	5	1	4	2	3	5	1
	loss	4	3	1	5	2	4	3	1	5	2
Varying	Tr	4	4	3	2	1	4	4	3	2	1
	Acc	5	3	4	2	1	5	4	3	2	1
	Total loss	5	2	4	3	1	5	2	4	3	1
EN50530	Total loss	5	2	4	3	1	5	2	4	3	1

Note: the light red parts indicate the methods with the best PI under a single test condition; the methods with the worst PI are marked in light green.

5. Conclusions

A neural network assisted VSS IncCond MPPT method with adaptive scaling factor for rapidly irradiance changing conditions is proposed in this study. Using any two operating points on the characteristic curves, an optimal scaling factor can be acquired using the proposed neural network to enhance the performance of conventional VSS IncCond MPPT technique. Experimental results show that the proposed method performs well both under varying irradiance condition and EN50530 testing conditions. Comparing with P&O, α -P&O, golden section and conventional VSS IncCond MPPT methods, the averaged tracking time/total tracking loss can be improved by 78.84%/45.59%, 78.84%/6.67%, 56.00%/45.30%, and 42.10%/39.49% under the tested varying irradiance condition. In addition, the proposed method can achieve the highest averaged tracking accuracy. Moreover, the tracking loss can be reduced by 95.58%, 42.51%, 93.66%, and 66.14% under EN50530 testing condition. The significant contribution of this study is that fast and accurate tracking can be accomplished without the demand for extra expensive irradiance and temperature sensors. The proposed method is uncomplicated; it can be integrated effortlessly into conventional VSS IncCond MPPT algorithms, allowing the developed MPPT solution to be more applicable for solar generation system applications.

Author Contributions: S.-P.Y., Y.-H.L., C.-Y.L., K.-C.H. and Y.-F.L. made considerable contributions in this research, S.-P.Y. and Y.-H.L. proposed ideas and research concepts at the beginning of the study, S.-P.Y. and C.-Y.L. completed the construction of the simulation platform and the construction of the experimental platform during the research process. All authors have read and agreed to the published version of the manuscript.

Funding: This research received no external funding.

Conflicts of Interest: The authors declare no conflict of interest.

References

1. Tazay, A.F.; Ibrahim, A.M.A.; Noureldeen, O.; Hamdan, I. Modeling, control, and performance evaluation of grid-tied hybrid PV/wind power generation system: Case study of Gabel El-Zeit region, Egypt. *IEEE Access* **2020**, *8*, 96528–96542. [CrossRef]
2. Shi, Z.; Guo, Y.; Li, P.; Sun, H. A boost CLLC converter controlled by PWM and PFM hybrid modulation for photovoltaic power generation. *IEEE Access* **2020**, *8*, 112015–112026. [CrossRef]
3. Kuzlu, M.; Cali, U.; Sharma, V.; Guler, O. Gaining insight into solar photovoltaic power generation forecasting utilizing explainable artificial intelligence tools. *IEEE Access* **2020**, *198*, 187814–187823. [CrossRef]
4. Chen, P.C.; Chen, P.Y.; Liu, Y.H.; Chen, J.H.; Luo, Y.F. A comparative study on maximum power point tracking techniques for photovoltaic generation systems operating under fast changing environments. *Sol. Energy* **2015**, *119*, 261–276. [CrossRef]

5. Karami, N.; Moubayed, N.; Outbib, R. General review and classification of different MPPT Techniques. *Renew. Sustain. Energy Rev.* **2017**, *68*, 1–18. [[CrossRef](#)]
6. Teng, J.H.; Huang, W.H.; Hsu, T.A.; Wang, C.Y. Novel and fast maximum power point tracking for photovoltaic generation. *IEEE Trans. Ind. Electron.* **2016**, *63*, 4955–4966. [[CrossRef](#)]
7. Başoğlu, M.E. A fast GMPPT algorithm based on PV characteristic for partial shading conditions. *Electronics* **2019**, *8*, 1142. [[CrossRef](#)]
8. Na, W.; Chen, P.; Kim, J. An improvement of a fuzzy logic-controlled maximum power point tracking algorithm for photovoltaic applications. *Appl. Sci* **2017**, *7*, 326. [[CrossRef](#)]
9. Doostabad, H.H.; Keypour, R.; Khalghani, M.R.; Khooban, M.H. A new approach in MPPT for photovoltaic array based on Extremum Seeking Control under uniform and non-uniform irradiances. *Sol. Energy* **2013**, *94*, 28–36. [[CrossRef](#)]
10. Kchaou, A.; Naamane, A.; Koubaa, Y.; Msirdi, N. Second order sliding mode-based MPPT control for photovoltaic applications. *Solar Energy* **2017**, *155*, 758–769. [[CrossRef](#)]
11. Khan, R.; Khan, L.; Ullah, S.; Sami, I.; Ro, J.S. Backstepping based super-twisting sliding mode MPPT control with differential flatness oriented observer design for photovoltaic system. *Electronics* **2020**, *9*, 1543. [[CrossRef](#)]
12. Mahmoud, Y.; Abdelwahed, M.; Saadany, E.F.E. An enhanced MPPT method combining model-based and heuristic techniques. *IEEE Trans. Sustain. Energy* **2016**, *7*, 576–585. [[CrossRef](#)]
13. Li, X.; Wen, H.; Jiang, L.; Xiao, W.; Du, Y.; Zhao, C. An improved MPPT method for PV system with fast-converging speed and zero oscillation. *IEEE Trans. Ind. Appl.* **2016**, *52*, 5051–5064. [[CrossRef](#)]
14. Koad, R.B.A.; Zobaa, A.F.; Shahat, A.E. A novel MPPT algorithm based on particle swarm optimization for photovoltaic systems. *IEEE Trans. Sustain. Energy* **2017**, *8*, 468–476. [[CrossRef](#)]
15. Rujula, A.A.B.; Abian, J.A.C. A novel MPPT method for PV systems with irradiance measurement. *Sol. Energy* **2014**, *109*, 95–104. [[CrossRef](#)]
16. Fathabadi, H. Novel fast dynamic MPPT (maximum power point tracking) technique with the capability of very high accurate power tracking. *Energy* **2016**, *94*, 466–475. [[CrossRef](#)]
17. Pandey, A.; Dasgupta, N.; Mukerjee, A.K. High performance algorithms for drift avoidance and fast tracking in solar MPPT system. *IEEE Trans. Energy Convers.* **2008**, *23*, 681–689. [[CrossRef](#)]
18. Liu, F.; Duan, S.; Liu, F.; Liu, B.; Kan, Y. A variable step size INC MPPT method for PV systems. *IEEE Trans. Ind. Electron.* **2008**, *55*, 2622–2628.
19. Lalili, D.; Mellit, A.; Lourci, N.; Medjahed, B.; Berkouk, E.M. Input output feedback linearization control and variable step size MPPT algorithm of a grid-connected photovoltaic inverter. *Renew. Energy* **2011**, *36*, 3282–3291. [[CrossRef](#)]
20. Mei, Q.; Shan, M.; Liu, L.; Guerrero, J.M.; Kan, Y. A novel improved variable step-size incremental resistance MPPT method for PV systems. *IEEE Trans. Ind. Electron.* **2010**, *58*, 2427–2434. [[CrossRef](#)]
21. Jiang, Y.; Qahouq, J.A.A.; Haskew, T.A. Adaptive step size with adaptive-perturbation-frequency digital MPPT controller for a single-sensor photovoltaic solar system. *IEEE Trans. Power Electron.* **2012**, *28*, 3195–3205. [[CrossRef](#)]
22. Lalili, D.; Mellit, A.; Lourci, N.; Medjahed, B.; Boubakir, C. State feedback control and variable step size MPPT algorithm of three level grid connected photovoltaic inverter. *Sol. Energy* **2013**, *98*, 561–571. [[CrossRef](#)]
23. Killi, M.; Samanta, S. An adaptive voltage sensor based MPPT for photovoltaic systems with SEPIC converter including steady-state and drift analysis. *IEEE Trans. Ind. Electron.* **2015**, *62*, 7609–7619. [[CrossRef](#)]
24. Shi, Y.; Li, R.; Xue, Y.; Li, H. High frequency link based grid tied PV system with small DC-link capacitor and low-frequency ripple-free maximum power point tracking. *IEEE Trans. Power Electron.* **2015**, *31*, 328–339. [[CrossRef](#)]
25. Loukriz, A.; Haddadi, M.; Messalti, S. Simulation and experimental design of a new advanced variable step size Incremental Conductance MPPT algorithm for PV systems. *ISA Trans.* **2016**, *62*, 30–38. [[CrossRef](#)]
26. Amir, A.; Amir, A.; Selvaraj, J.; Rahim, N.A.; Abusorrah, A.M. Conventional and modified MPPT techniques with direct control and dual scaled adaptive step-size. *Sol. Energy* **2017**, *157*, 1017–1031. [[CrossRef](#)]
27. Thangavelu, A.; Vairakannu, S.; Parvathyshankar, D. Linear open circuit voltage variable step size incremental conductance strategy based hybrid MPPT controller for remote power applications. *IET Power Electron* **2017**, *10*, 1363–1376. [[CrossRef](#)]
28. Zhu, Y.; Fei, J. Adaptive global fast terminal sliding mode control of grid-connected photovoltaic system using fuzzy neural network approach. *IEEE Access* **2017**, *5*, 9476–9484. [[CrossRef](#)]
29. Chandra, S.; Gaur, P.; Pathak, D. Radial basis function neural network based maximum power point tracking for photovoltaic brushless DC motor connected water pumping system. *Comput. Electr. Eng.* **2020**, *86*, 106730. [[CrossRef](#)]
30. Punitha, K.; Devaraj, D.; Sakthivel, S. Artificial neural network based modified incremental conductance algorithm for maximum power point tracking in photovoltaic system under partial shading conditions. *Energy* **2013**, *62*, 330–340. [[CrossRef](#)]
31. Issaadi, S.; Issaadi, W.; Khireddine, A. New intelligent control strategy by robust neural network algorithm for real time detection of an optimized maximum power tracking control in photovoltaic systems. *Energy* **2019**, *187*, 115881. [[CrossRef](#)]
32. Majidi, S.D.A.; Abbod, M.F.; Raweshidy, H.S.A. A particle swarm optimisation-trained feedforward neural network for predicting the maximum power point of a photovoltaic array. *Eng. Appl. Artif. Intell.* **2020**, *92*, 103688. [[CrossRef](#)]
33. Subiyanto, S.; Mohamed, A.; Hannan, M.A. Intelligent maximum power point tracking for PV system using Hopfield neural network optimized fuzzy logic controller. *Energy Build.* **2012**, *51*, 29–38. [[CrossRef](#)]

34. Kofinas, P.; Dounis, A.I.; Papadakis, G.; Assimakopoulos, M.N. An intelligent MPPT controller based on direct neural control for partially shaded PV system. *Energy Build.* **2015**, *90*, 51–64. [[CrossRef](#)]
35. Ammar, M.B.; Chaabene, M.; Chtourou, Z. Artificial neural network based control for PV/T panel to track optimum thermal and electrical power. *Energy Convers. Manag.* **2013**, *65*, 327–380. [[CrossRef](#)]
36. Kassem, A.M. MPPT control design and performance improvements of a PV generator powered DC motor-pump system based on artificial neural networks. *Int. J. Electr. Power Energy Syst.* **2012**, *43*, 90–98. [[CrossRef](#)]
37. Majidi, S.D.A.; Abbod, M.F.; Raweshidy, H.S.A. Design of an efficient maximum power point tracker based on ANFIS using an experimental photovoltaic system data. *Electronics* **2019**, *8*, 858. [[CrossRef](#)]
38. Liu, Y.H.; Chen, J.H.; Huang, J.W. Global maximum power point tracking algorithm for PV systems operating under partially shaded conditions using the segmentation search method. *Sol. Energy* **2014**, *103*, 350–363. [[CrossRef](#)]
39. Kheldoun, A.; Bradai, R.; Boukenoui, R.; Mellit, A. A new Golden Section method-based maximum power point tracking algorithm for photovoltaic systems. *Energy Convers. Manag.* **2016**, *111*, 125–136. [[CrossRef](#)]